ISSN 0030-400X, Optics and Spectroscopy, 2020, Vol. 128, No. 7, pp. 1018–1025. © Pleiades Publishing, Ltd., 2020.
Russian Text © The Author(s), 2020, published in Optika i Spektroskopiya, 2020, Vol. 128, No. 7, pp. 1012–1019.

UV, IR, AND TERAHERTZ OPTICS

Emission Efficiency of Terahertz Antennas with Conventional Topology and Metal Metasurface: A Comparative Analysis

D. V. Lavrukhin[a, b, *], A. E. Yachmenev[a], I. A. Glinskiy[a], N. V. Zenchenko[a, b], R. A. Khabibullin[a], Yu. G. Goncharov[c], I. E. Spektor[c], K. I. Zaytsev[b, c], and D. S. Ponomarev[a]

[a] *Institute of Ultrahigh-Frequency Semiconductor Electronics, Russian Academy of Sciences, Moscow, 117105 Russia*
[b] *Bauman Moscow State Technical University, Moscow, 105005 Russia*
[c] *Prokhorov General Physics Institute, Russian Academy of Sciences, Moscow, 119991 Russia*
**e-mail: denis_lavruhin@mail.ru*

Received December 17, 2019; revised January 10, 2020; accepted February 28, 2020

Abstract—Characteristics of photoconductive antennas (PCAs)—radiation sources with conventional topology and a metal metasurface in the shape of a plasmonic grating made on the basis of InGaAs/InAlAs superlattice heterostructures—have been studied experimentally. The photocurrents and THz power spectra of samples of PCAs have been measured, the energy characteristics of terahertz (THz) radiation, and the optical-to-THz conversion efficiency at different bias voltages and average laser excitation power have been determined. For PCAs with a metasurface, the integrated THz radiation power of 10 μW and a conversion efficiency of up to 0.2%, unattainable for antennas with conventional topology due to their thermal breakdown, have been demonstrated experimentally. Therefore, it can be stated that PCAs with a metasurface are efficient sources of THz radiation and can become an element base for constructing THz spectroscopy systems associated with solving medical diagnostic problems.

Keywords: terahertz pulsed spectroscopy, element base of terahertz optics, photoconductive antenna, plasmonic grating, metasurface, optical field plasmon localization, semiconductors, noninvasive medicine

DOI: 10.1134/S0030400X20070103

INTRODUCTION

The application of methods of terahertz (THz) pulsed spectroscopy and imaging to solve applied problems of medical diagnosis of malignant neoplasms of various nosology and localization has recently become increasingly relevant [1–4]. As achievements, one can indicate the possibility of using THz technologies in problems of early noninvasive and intraoperative diagnostics of malignant tumors of skin and mucosa [5–9], minimally invasive and intraoperative diagnostics of intestinal [10, 11] and stomach [12] neoplasms, as well as intraoperative diagnosis of breast [13–15] and brain [16–19] tumors. Due to the possibility of simultaneous obtaining information on the amplitude and phase of electromagnetic waves that were reflected from or transmitted through an object of study, coherent (pulsed) methods of generation and detection of THz radiation are most promising approach to solving problems of medical diagnostics [3, 20]. Such systems efficiently operate at room temperature ensuring the dynamic range of up to 110 dB [21] in the frequency range between 0.1 and 4.5 THz.

Photoconductive antennas (PCAs) based on GaAs and its ternary compounds are the most widespread sources and detectors of radiation in THz pulsed systems. It should be noted that a rather large band gap in GaAs (E_g = 1.42 eV) implies the use of a complex and bulky optical system pumped by radiation from a Ti:Sapphire laser with a central wavelength of 800 nm. In this case, $In_xGa_{1-x}As$ solid solutions make it possible to operate (depending on molar fraction x of indium) with IR laser pumping in the wavelength range 1.03–1.56 μm emitted by compact and inexpensive fiber laser systems. Unfortunately, InGaAs layers have rather low electrical resistance and large lifetimes of photoexcited charge carriers, which greatly complicates their widespread use in THz spectroscopy systems and, in particular, in PCAs on their basis. The authors of many foreign studies have made various attempts to improve the above-indicated characteristics of InGaAs, for example, by ion implantation [22, 23] or low-temperature growth with compensating doping [24–26]. However, the epitaxial growth of InGaAs/InAlAs photoconductive superlattice heterostructures (SLs) proved to be the most successful among other approaches. Depending on the applica-

tion, these heterostructures can be divided into the following three groups.

(i) InGaAs/InAlAs SLs doped with erbium atoms. These structures have extremely short lifetimes of photoexcited charge carriers, with their mobilities being relatively high; therefore, these structures can be used both in PCA-emitters and PCAs detectors [27].

(ii) InGaAs/InAlAs SLs grown at lowered temperatures with additional doping of InGaAs photoconductive layers by beryllium atoms. These structures have ultrashort lifetimes of photoexcited carriers and are excellent for use in PCA detectors [26].

(iii) Lattice-matched and strained undoped InGaAs/InAlAs SLs with InAlAs barrier layers grown at lowered temperatures. Photoexcited carriers in such structures have rather high mobilities and relatively short lifetimes. These structures are used in PCA-emitter [28, 29].

It is important to note that the dynamic range of pulsed THz spectroscopy systems is largely determined by the parameters of the PCA-emitter. Because the average IR radiation power of compact fiber lasers for the excitation of PCAs is ~10 mW, this imposes a fundamental limitation on the minimum efficiency of optical–THz energy conversion in PCAs [30, 31]. To date, the most successful method for increasing the conversion efficiency is the formation of a dielectric or metal metasurface in the PCA gap [32]. In particular, metasurfaces in the shape of metal plasmonic electrodes noticeably enhance the localization of the laser pump radiation in the contact region between the grating metal and the photoconductive layer and, correspondingly, increasing the effective absorption of the laser radiation in the photoconductive layer [33]. The grating efficiency was shown to increase proportionally to its aspect ratio, i.e., to the ratio of the height of a single plasmonic electrode to the period of the grating [34–36]. Technological limitations on the maximum thickness of the electron resist layer, as well as the need to compensate effects associated with the proximity of adjacent electrodes when exposing the electronic resist, lead to the situation that the larger the aspect ratio, the more expensive is the grating and the more difficult becomes its fabrication.

Another way to increase the efficiency is related to the selection of pump photons energy for PCAs. It is known that, if narrowband SLs are pumped by the laser radiation in the range 780–800 nm, photoexcited ("hot") charge carriers experience strong intervalley scattering, and their lifetimes somewhat increase [37, 38]. However, it was shown that, in this case, a higher absorption coefficient enhances the localization of the optical pulse energy near the surface of the photoconductive layer/electrodes. In other words, in some cases [38, 39], a higher photon energy can provide a higher integrated power of the THz radiation compared to the excitation near the bottom of the conduction band of the photoconductive layer.

In this work, we will combined several approaches to increase the antenna efficiency: the fabrication of narrow-gap InGaAs/InAlAs SLs with ultrashort lifetimes of excited charge carriers in InGaAs photoconductive layers, fabrication of PCA-emitters with high aspect ratio plasmonic electrodes based on SLs, and excitation of a narrow-gap material by the visible radiation. Based on the results of comparative measurements of average photocurrents, integrated THz radiation powers, and optical–THz conversion efficiencies (for different values of the average laser pump power and applied bias voltage), we determined the modes in which PCAs with conventional topology can compete with PCAs with a metasurface (plasmonic grating).

SAMPLES AND INVESTIGATION METHODS

In experiments, we compared samples of PCAs with conventional bowtie topology and having the bowtie with a metasurface (plasmonic grating) topology based on InGaAs/InAlAs SLs with ultrashort lifetimes of photoexcited charge carriers, which were designed and fabricated at the Institute of Ultra-high Frequency Semiconductor Electronics of the Russian Academy of Sciences. The photoconductive gap of the PCAs of both types was 10 μm. Narrowband 30-period $In_{0.53}Ga_{0.47}As/In_{0.52}Al_{0.48}As$ SLs were formed on GaAs substrates by the method of molecular beam epitaxy with a step-graded metamorphic buffer [40]. Prior to the deposition of the electrodes, the SLs surface was coated with a 230-nm Si_3N_4 layer in which windows were etched by the optical photolithography method to ensure electrical contacts between the antenna electrodes and the SLs surface. The topology of the electrodes was formed using the method of lift-off photolithography of the deposited system of Ti/Au metals (50 nm/450 nm). To create a metasurface using the method of electron-beam lift-off lithography of a Ti/Au (18 nm/82 nm) metal system, a metal grating was formed, the electrode height and the width and the gap between two adjacent electrodes of which were equal to 100 nm (the aspect ratio between the electrode height and the period was 1 : 2). Finally, a 180-nm thick Al_2O_3 antireflection layer was deposited on the surface of the PCA. The fabrication technology for antenna samples was described in detail in [41–44].

The emission spectra of PCA samples at different average laser pump powers and applied bias voltages were recorded using an original THz pulsed spectrometer in the time domain [44, 45]. The PCA was used as a radiation source, while a commercial TERRA-8 PCA (Menlo Systems) served as a detector. Alternating bias voltage U_b was applied to the PCA-emitter. The bias amplitude could be varied in the range of 5–33 V, while the pulse repetition rate was constant and equal to 10 kHz. After preliminary amplification, the current signal from the TERRA-8 PCA detector was

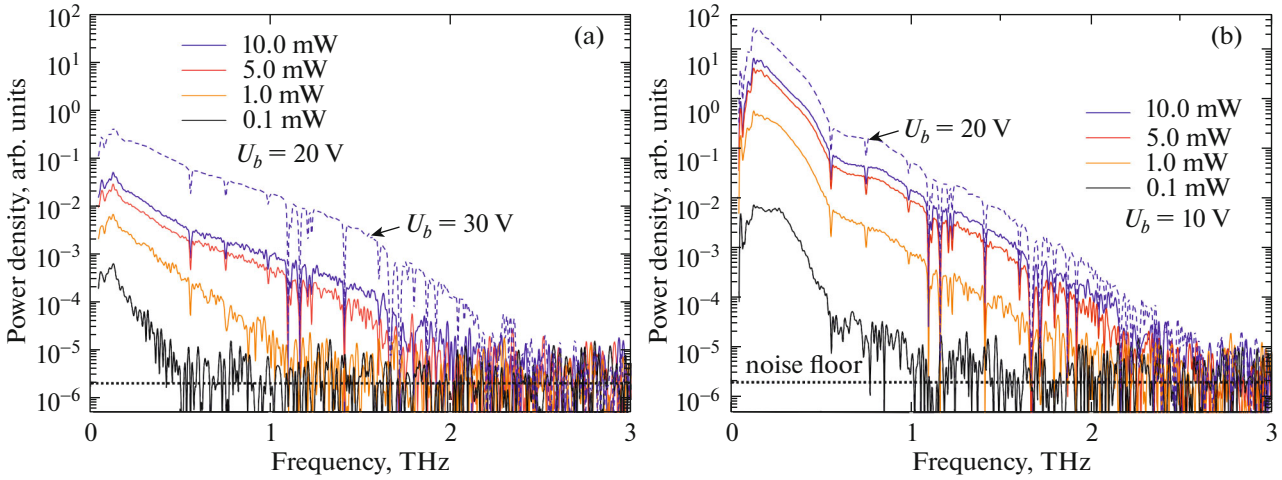

Fig. 1. THz emission spectra of PCAs with (a) conventional topology and (b) metasurface (plasmonic grating) at different laser pump average powers.

synchronously demodulated at this frequency, which made it possible to ensure a high signal-to-noise ratio of ~80 dB. Both PCAs were pumped with ultrashort pulses from an EFOA-SH fiber laser (Avesta-Proekt) with the following parameters: the central wavelength was 780 nm, the pulse repetition frequency was f_L = 65 MHz, and the pulse duration was ~85 fs. The average power of the laser radiation in the probe beam was fixed at a level of ~10 mW. In the pump beam, using an adjustable attenuator, the average power was varied in the range P_{opt} = 0.1–10.0 mW. When pumping antennas with a metasurface, the polarization vector of the light wave was oriented perpendicularly to the grating electrodes. To match the PCA-emitter and the PCA detector with free space, we used hyper-hemispherical lenses made of high-resistivity silicon (high-resistivity float-zone silicon-HRFZ-Si). The lens diameter was 10 mm and their height was 6.7 mm; the THz radiation was collected and transported with off-axis parabolic mirrors with a diameter of 2 inch and a focal length of 4 inch. The registration time of the THz radiation spectrum of one PCA sample with a frequency resolution of ~0.02 THz for the spectrometer was ~30 s. This was achieved, among other things, because of the use of a fast 150-mm stage in the optical delay line with a linear actuator equipped with feedback by the carriage position (by optical encoder).

Average photocurrents i_{ph} for the studied samples of PCAs in the voltage range U_b = 1–70 V were measured with a microammeter in the antenna's electric circuit. The integrated power P_{THz} of THz radiation was measured by absolutely calibrated Golay cell, which was installed in an close proximity of the matching Si lens for the studied sample of the PCA emitter. Because of slow response of the Golay cell, in these measurements the laser radiation in the pump beam was modulated by a mechanical chopper at a frequency of 23 Hz. The efficiencies of optical–THz conversion in samples of PCA-emitters were calculated by measuring the integrated radiation powers according to the expression $\eta = P_{THz}/P_{opt}$.

RESULTS AND DISCUSSION

The generation spectra of the studied samples are shown in Fig. 1. It was found that, at the same bias voltages, the signals from the PCA samples with conventional topology are significantly weaker; therefore, their spectra were recorded using voltages $U_b \geq 20$ V. It can be seen that, the spectral radiation density for PCAs with the metasurface and for PCAs with conventional topology is distributed over a wide frequency range and exceeds the noise level of the spectrometer up to frequences 2.5–3.0 THz. A particular feature of PCAs with the metasurface is a significant increase in the power in the low-frequency range of the spectrum down to 0.5 THz. It should be noted that PCAs with conventional topology exhibit a decay of the high-frequency edge of the spectrum with decreasing average laser power, while, for PCAs with the metasurface, the shape of the spectra does not depend neither on the applied bias voltage nor on the average laser power.

The typical dependences of the average photocurrent on the bias voltage applied to the antenna for samples of PCA-emitters with conventional topology and metasurface are shown in Fig. 2a. It can be seen that, although the band gap of $In_{0.53}Ga_{0.47}As$ layers is small, being ~0.9 eV, in the case of conventional topology of the electrodes, the breakdown of PCAs does not occur at voltages of up to U_b = 60 V (E_b = 60 kV/cm), with the photocurrent reaching values of ~1 mA. The formation of a metasurface leads to that the distribution

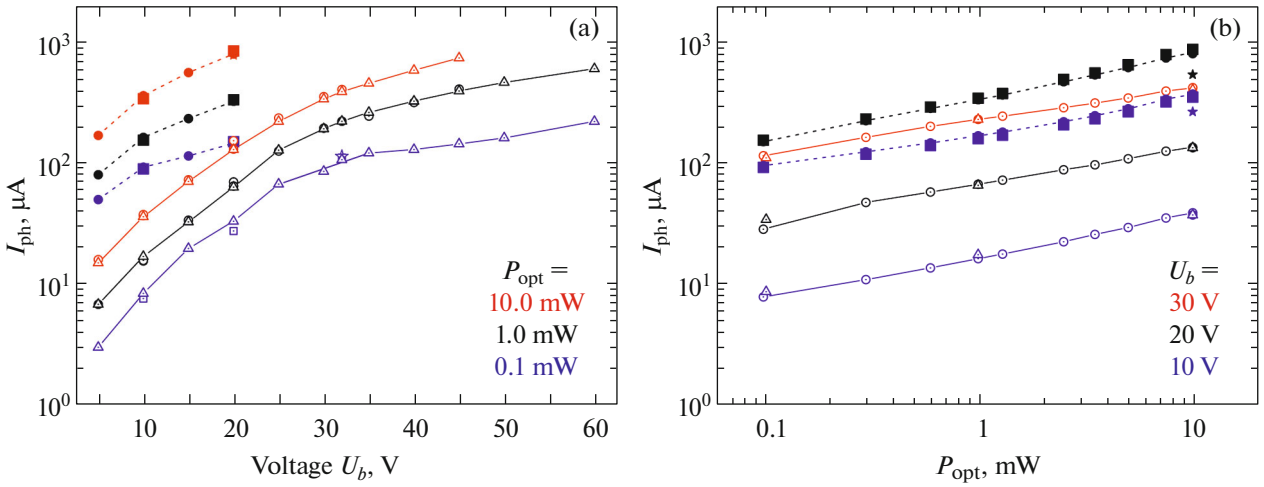

Fig. 2. Photocurrents of PCAs samples under different laser pumping conditions: (a) at fixed laser pump average power P_{opt} and (b) at fixed bias voltage U_b. Solid curves refer to a PCA with conventional topology, while dashed curves correspond to a PCA with metasurface (plasmonic grating).

of the electric field strength in the gap becomes inhomogeneous; therefore, even without the laser pumping, the breakdown of the antenna can occur even at $U_b = 30$ V.

Measurements by the optical pump–probe method showed that, for the pump regimes that were selected for the used SLs, the lifetimes of photoexcited charge carriers are $\tau_c \sim 5$ ps [40]. During these times, only a small fraction of photoexcited carriers, proportional to the average drift velocity, can reach metal contacts. In experiments with these samples, for all laser pump powers, the photocurrent increased according to a power law with increasing bias voltage (Fig. 3a, solid lines). In the case of a metasurface, photoexcited carriers are localized near the contact between the grating metal and the semiconductor; therefore, in experiments, the photocurrents change little with voltage and rapidly reach values typical of saturation in conventional topology (Fig. 2a, dashed lines). It should be noted that, for thin $In_{0.53}Ga_{0.47}As$ layers, the dependence of the carrier drift velocity on the applied voltage will differ from the bulk case, because, among other things, of a decrease in the relaxation time of their momentum due to scattering by heterointerfaces.

The measured dependences of the photocurrents on the average laser power are shown in Fig. 2b. For conventional topology, the curve at $U_b = 30$ V corresponds to the case in which, for the given pump value, a maximum possible number of charge carriers reaches the antenna electrodes. In the case of the metasurface, photoexcited carriers reach the antenna electrodes much easier, and the bias voltage affects the photocurrent to a lesser degree, and the experimental curves repeat in general the dependence for the case of the maximum applied voltage in conventional topology. It can be easily verified that, at an average laser radiation power of $P_{opt} \sim 1$ mW, the concentration of photoexcited charge carriers in the SL is too low to screen the electric bias field applied to the antenna gap by charges separated in space [44]. At $P_{opt} > 1$ mW, the experimental curves for samples of PCAs of both types do not change their character; therefore, the signal saturation effect due to a high level of optical pumping can be neglected in the entire considered range of the pump power.

The dependences of integrated powers P_{THz} of the THz radiation of the PCAs and of optical–THz conversion efficiencies η in the antennas on the applied bias voltage and pump power are shown in Figs. 3 and 4, respectively. It was shown in [46, 47] that the maximum integrated power of the THz radiation of an PCA is limited by the energy of the antenna stored in the gap. For estimates, neglecting the effect of matching the impedances of the photoconductor and the antenna on the power transmission to the antenna [44], we can assume that $P_{max} \sim (U_b^2/R_a)f_L\tau_{THz}$, where the total duration of the THz signal is $\tau_{THz} \sim 3R_aC_a \sim 1$ ps, while R_a is the real part of the antenna impedance for frequencies up to ~1.5–2.0 THz, and C_a is the capacity of the antenna gap. Correspondingly, for typical values of $U_b = 10$ V and $R_a = 70$ Ω (for the bowtie antenna [48]), the maximum integrated power is $P_{max} \sim 400$ μW. The values of the integrated power determined in all experiments do not exceed 10 μW ($P_{THz} \ll P_{max}$); i.e., although the average photocurrent is significant, ~1 mA, the measurements are carried out in the mode of weak laser pumping. In this case, the complex character of the dependence $P_{THz}(U_b)$ is not associated with surmounting the screening effect of photoexcited current carriers, but, rather, is likely determined by the dependence of the drift velocity of

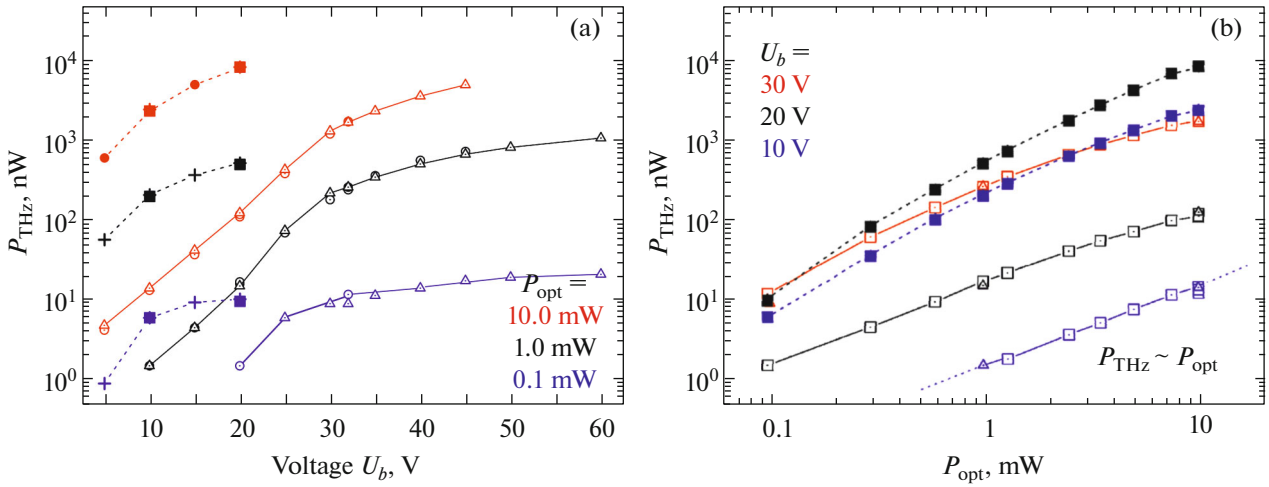

Fig. 3. Integrated power of THz radiation of samples of PCAs under different laser pumping conditions: (a) at fixed laser pump average power P_{opt} and (b) at fixed bias voltage U_b. Solid curves refer to a PCA with conventional topology, while dashed curves correspond to a PCA with metasurface (plasmonic grating).

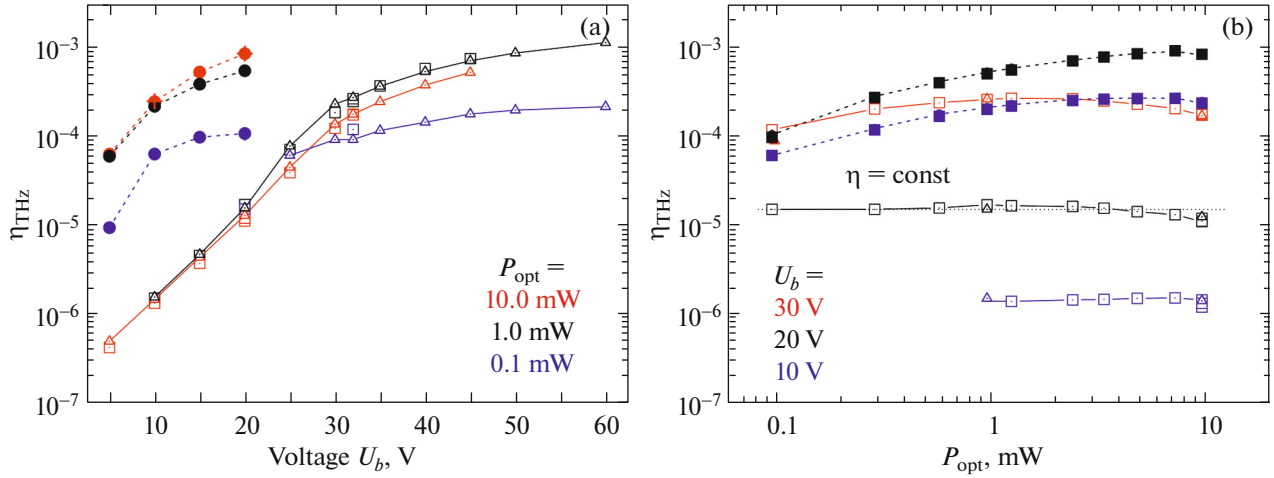

Fig. 4. Optical-to-THz conversion efficiency of samples of PCAs under different laser pumping conditions: (a) at fixed laser pump average power P_{opt} and (b) at fixed bias voltage U_b. Solid curves refer to a PCA with conventional topology, while dashed curves correspond to a PCA with metasurface (plasmonic grating).

these carriers on the applied bias voltage in the narrow-gap material of the SL ($In_{0.53}Ga_{0.47}As$).

Comparison of the THz measurement results for the PCAs with conventional topology and metasurface, which are shown in Fig. 4a, shows that, for the same applied voltage, the efficiency and the integrated radiation power of an antenna with a metasurface is always higher, although the lower conversion efficiency in conventional antenna can be compensated to some extent by increasing the voltage. An electrical breakdown of the bulk material $In_{0.53}Ga_{0.47}As$ occurs at field strengths of ~200 kV/cm [49] (U_b = 200 V); however, in practice, even half of this value cannot be achieved. The contribution from the leakage current (dark current) to the total antenna current rapidly increases and, at U_b = 60 V, reaches values of ~230 μA for the samples under study (at a photocurrent of ~1 mA), which sharply shortens the lifetime of PCAs and, subsequently, leads to thermal breakdown of the antenna.

It can be seen from Fig. 4b that, for PCAs with conventional topology, $P_{THz} \sim P_{opt}^n \sim P_{opt}$. A decrease in exponent n of the power-law dependence of the integrated THz power on the pump power (in our case, to

$n = 1$) compared with the value $n = 2$, which is expected from general considerations, the authors of [46, 47] attribute to saturation effects. In the case of SLs, it is likely that the role is played by the saturation of trap states (trapping centers), which ensure ultrashort lifetimes of photoexcited carriers in $In_{0.53}Ga_{0.47}As$, which, in turn, is associated with a lower density of trapping centers in comparison with the cases of formation of the same centers due to ion implantation or compensating doping [22–26]. We note that this remark is also valid with respect to the weak dependence of the average photocurrent on the pump power.

Since exponent n is low, it is hardly expedient to compensate the low integrated power of the THz radiation by increasing the laser pump power, because, among other things, of the passage to the high pumping mode, i.e., due to reducing of the optical–THz conversion efficiency due to electric-field screening. It is most likely that precisely the screening of the external electric field explains the dependence of the emitted THz power on the laser pumping for $U_b = 30$ V even at $P_{opt} > 5$ mW in an antenna with conventional topology (Fig. 3b). Therefore, if solving applied problems of medical diagnostics requires the use of integrated powers of the THz radiation at a level of ~5–10 μW, then PCAs with a metasurface should be used as radiation sources. At power levels of ~1–5 μW or lower, the advantages of PCAs with the metasurface as compared to PCAs with conventional topology become insignificant.

As a result, we found that the optical–THz conversion efficiency for PCAs with conventional topology does not exceed $\eta = 0.1\%$ (for $U_b = 50$ V). From a comparison of the η values in Fig. 4a, we can conclude that PCAs with conventional topology can compete with PCAs with a metasurface, but only upon their operation in a mode close to the antenna thermal breakdown. At the same time, the conversion efficiency in PCAs with a metasurface tends to a subsequent increase both with the voltage and the pump power. In particular, at $U_b = 30$ V and $P_{opt} = 3.4$ mW, we succeeded in achieving $\eta = 0.2\%$ with a relatively safe photocurrent for the antenna of $i_{ph} = 0.9$ mA.

CONCLUSIONS

In this paper, we considered several approaches to increase the efficiency of photoconductive antennas PCAs-emitters—the fabrication of InGaAs/InAlAs photoconductive superlattice heterostructures with ultrashort lifetimes of photoexcited charge carriers; fabrication of PCAs with conventional topology and with a metasurface (plasmonic gratings with a high aspect ratio) based on these heterostructures; and excitation of narrow-gap material by visible radiation from the femtosecond laser.

For samples of PCAs, average photocurrents, integrated THz radiation powers, and the efficiencies of converting laser radiation energy into electromagnetic oscillations of the THz range were measured for different average laser pump powers and applied bias voltages. The use of a metasurface made it possible to achieve values of the integrated radiation power THz of ~10 μW at a voltage of 20 V and an average laser pump power of 10 mW. The maximum conversion efficiency was $\eta = 0.2\%$, which is unattainable for PCAs with conventional topology due to their thermal breakdown. This is mainly related to the difference between the emission spectra of the antennas for frequencies lower than 0.5 THz. A comparative analysis showed that, for solving applied problems which require integrated radiation THz powers at a level of ~5–10 μW, PCAs with a metasurface should be used as radiation sources, while, for the power level of ~1–5 μW or lower, the advantages of PCAs with the metasurface over PCAs with conventional topology become insignificant.

FUNDING

This work was financially supported by the Russian Science Foundation (grant no. 19-79-10240).

CONFLICT OF INTEREST

The authors declare that they have no conflict of interest.

REFERENCES

1. K. I. Zaytsev, I. N. Dolganova, N. V. Chernomyrdin, G. M. Katyba, A. A. Gavdush, O. P. Cherkasova, G. Komandin, M. A. Shchedrina, A. N. Khodan, D. S. Ponomarev, I. V. Reshetov, V. Karasik, M. Skorobogatiy, V. N. Kurlov, and V. V. Tuchin, J. Opt. **22**, 013001 (2019).

2. Q. Sun, Y. He, K. Liu, S. Fan, E. P. Parrott, and E. Pickwell-MacPherson, Quant. Imag. Med. Surg. **7**, 345 (2017).

3. X. Yang, X. Zhao, K. Yang, Y. Liu, Y. Liu, W. Fu, and Y. Luo, Trends Biotechnol. **34**, 810 (2016).

4. O. A. Smolyanskaya, N. V. Chernomyrdin, A. A. Konovko, K. I. Zaytsev, I. A. Ozheredov, O. P. Cherkasova, M. M. Nazarov, J. P. Guilleti, S. A. Kozlova, Yu. V. Kistenev, J.-L. Coutaz, P. Mounaix, V. L. Vaks, J.-H. Son, H. Cheon, V. P. Wallac, Yu. Feldman, N. I. Popov, and V. V. Tuchin, Prog. Quantum Electron. **62**, 1 (2018).

5. R. M. Woodward, V. P. Wallace, R. J. Pye, B. E. Cole, D. D. Arnone, E. H. Linfield, and M. Pepper, J. Invest. Dermatol. **120**, 72 (2003).

6. V. P. Wallace, A. J. Fitzgerald, S. Shankar, N. Flanagan, R. Pye, J. Cluff, and D. D. Arnone, Brit. J. Dermatol. **151**, 424 (2004).

7. C. S. Joseph, R. Patel, V. A. Neel, R. H. Giles, and A. N. Yaroslavsky, J. Biophoton. **7**, 295 (2014).
8. K. I. Zaytsev, K. G. Kudrin, V. E. Karasik, I. V. Reshetov, and S. O. Yurchenko, Appl. Phys. Lett. **106**, 053702 (2015).
9. Y. Sim, J. Y. Park, K. M. Ahn, C. Park, and J. H. Son, Biomed. Opt. Express **4**, 1413 (2013).
10. C. B. Reid, A. Fitzgerald, G. Reese, R. Goldin, P. Tekkis, P. S. O'Kelly, and E. Pickwell-MacPherson, Phys. Med. Biol. **56**, 4333 (2011).
11. P. Doradla, K. Alavi, C. S. Joseph, and R. H. Giles, J. Biomed. Opt. **18**, 090504 (2013).
12. D. Hou, X. Li, J. Cai, Y. Ma, X. Kang, P. Huang, and G. Zhang, Phys. Med. Biol. **59**, 5423 (2014).
13. A. J. Fitzgerald, V. P. Wallace, M. Jimenez-Linan, L. Bobrow, R. J. Pye, A. D. Purushotham, and D. D. Arnone, Radiology **239**, 533 (2006).
14. P. C. Ashworth, E. Pickwell-MacPherson, E. Provenzano, S. E. Pinder, A. D. Purushotham, M. Pepper, and V. P. Wallace, Opt. Express **17**, 12444 (2009).
15. B. C. Q. Truong, H. D. Tuan, A. J. Fitzgerald, V. P. Wallace, and H. T. Nguyen, IEEE Trans. Biomed. Eng. **62**, 699 (2015).
16. S. Oh, S. H. Kim, Y. B. Ji, K. Jeong, Y. Park, J. Yang, D. W. Park, S. K. Noh, S. G. Kang, Y. M. Huh, J. H. Son, and J. S. Suh, Biomed. Opt. Express **5**, 2837 (2014).
17. Y. Ji, S. J. Oh, S. G. Kang, J. Heo, S. H. Kim, Y. Choi, S. Song, H. Y. Son, S. H. Kim, J. H. Lee, S. J. Haam, Y. M. Huh, J. H. Chang, C. Joo, and J. S. Suh, Sci. Rep. **6**, 36040 (2016).
18. S. Yamaguchi, Y. Fukushi, O. Kubota, T. Itsuji, T. Ouchi, and S. Yamamoto, Sci. Rep. **6**, 30124 (2016).
19. A. A. Gavdush, N. V. Chernomyrdin, K. M. Malakhov, S.-I. T. Beshplav, I. N. Dolganova, A. V. Kosyrkova, P. V. Nikitin, G. R. Musina, G. M. Katyba, I. V. Reshetov, O. P. Cherkasova, G. A. Komandin, V. E. Karasik, A. A. Potapov, V. V. Tuchin, and K. I. Zaytsev, J. Biomed. Opt. **24**, 027001 (2019). doi 1.JBO.24.2.027001
20. Y. S. Lee, *Principles of Terahertz Science and Technology* (Springer, US, 2009).
21. M. Yahyapour, A. Jahn, K. Dutzi, T. Puppe, P. Leisching, B. Schmauss, N. Vieweg, and A. Deninger, Appl. Sci. **9**, 1283 (2019). https://doi.org/10.3390/app9071283
22. R. Huber, A. Brodschelm, F. Tauser, and A. Leitenstorfer, Appl. Phys. Lett. **76**, 3191 (2000).
23. N. Chimot, J. Mangeney, P. Mounaix, M. Tondusson, K. Blary, and J. F. Lampin, Appl. Phys. Lett. **89**, 083519 (2006).
24. M. Suzuki and M. Tonouchi, Appl. Phys. Lett. **86**, 163504 (2005). https://doi.org/10.1063/1.1901817
25. B. Globisch, R. J. B. Dietz, R. B. Kohlhaas, T. Göbel, M. Schell, D. Alcer, M. Semtsiv, and W. T. Masselink, J. Appl. Phys. **121**, 053102 (2017). https://doi.org/10.1063/1.4975039
26. R. J. Dietz, B. Globisch, H. Roehle, D. Stanze, T. Göbel, and M. Schell, Opt. Express **22**, 19411 (2014).
27. F. Ospald, D. Maryenko, K. Klitzing, D. C. Driscoll, M. P. Hanson, H. Lu, A. C. Gossard, and J. H. Smet, Appl. Phys. Lett. **92**, 131117 (2008).
28. H. Roehle, R. J. B. Dietz, H. J. Hensel, J. Böttcher, H. Künzel, D. Stanze, M. Schell, and B. Sartorius, Opt. Express **18**, 2296 (2010).
29. D. S. Ponomarev, A. Gorodetsky, A. E. Yachmenev, S. S. Pushkarev, R. A. Khabibullin, M. M. Grekhov, K. I. Zaytsev, D. I. Khusyainov, A. M. Buryakov, and E. D. Mishina, J. Appl. Phys. **125**, 151605 (2019).
30. I. A. Glinskiy, R. A. Khabibullin, and D. S. Ponomarev, Russ. Microelectron. **46**, 408 (2017). https://doi.org/10.1134/S1063739717060051
31. N. Khiabani, Y. Huang, Y. Shen, and S. Boyes, IEEE Trans. Antennas Propag. **61**, 1538 (2013).
32. A. E. Yachmenev, D. V. Lavrukhin, I. A. Glinskiy, N. V. Zenchenko, Y. G. Goncharov, I. E. Spektor, R. A. Khabibullin, T. Otsuji, and D. S. Ponomarev, Opt. Eng. **59**, 061608 (2019). https://doi.org/10.1117/1.OE.59.6.061608
33. D. V. Lavrukhin, A. E. Yachmenev, I. A. Glinskiy, R. A. Khabibullin, Y. G. Goncharov, M. Ryzhii, T. Otsuji, I. E. Spector, M. Shur, M. Skorobogatiy, K. I. Zaytsev, and D. S. Ponomarev, AIP Adv. **9**, 015112 (2019). https://doi.org/10.1063/1.5081119
34. P. B. Catrysse, G. Veronis, H. Shin, J.-T. Shen, and S. Fan, Appl. Phys. Lett. **88**, 031101 (2006).
35. S. G. Park, Y. Choi, Y.-J. Oh, and K.-H. Jeong, Opt. Express **20**, 25530 (2012).
36. B. Y. Hsieh and M. Jarrahi, J. Appl. Phys. **109**, 084326 (2011).
37. R. Dietz, A. Brahm, A. Velauthapillai, A. Wilms, C. Lammers, B. Globisch, M. Koch, G. Notni, and M. Schell, J. Infrared Millim. Terahertz Waves **36**, 60 (2015).
38. R. J. B. Dietz, R. Wilk, and B. Globisch, J. Infrared Millim. Terahertz Waves **34**, 231 (2013).
39. O. Hatem, J. R. Freeman, and J. E. Cunningham, J. Infrared Millim. Terahertz Waves **37**, 415 (2016).
40. D. S. Ponomarev, R. A. Khabibullin, A. N. Klochkov, A. E. Yachmenev, A. S. Bugaev, D. I. Khusyainov, A. M. Buriakov, V. P. Bilyk, and E. Mishina, Semiconductors **52**, 864 (2018).
41. D. S. Ponomarev, R. A. Khabibullin, A. E. Yachmenev, A. Yu. Pavlov, D. N. Slapovskiy, I. A. Glinskiy, D. V. Lavrukhin, O. A. Ruban, and P. P. Maltsev, Semiconductors **51**, 1218 (2017).

42. D. V. Lavrukhin, G. M. Katyba, A. E. Yachmenev, R. R. Galiev, I. A. Glinskiy, R. A. Khabibullin, Y. G. Goncharov, I. E. Spektor, D. I. Khusyainov, A. M. Buryakov, E. D. Mishina, N. V. Chernomyrdin, K. I. Zaytsev, and D. S. Ponomarev, Proc. SPIE **10680**, 106801M (2018).

43. D. V. Lavrukhin, R. R. Galiev, A. Yu. Pavlov, A. E. Yachmenev, M. V. Maitama, I. A. Glinskii, R. A. Khabibullin, Yu. G. Goncharov, K. I. Zaitsev, and D. S. Ponomarev, Opt. Spectrosc. **126**, 580 (2019).

44. D. V. Lavrukhin, A. E. Yachmenev, A. Yu. Pavlov, R. A. Khabibullin, Yu. G. Goncharov, I. E. Spektor, G. A. Komandin, S. O. Yurchenko, N. V. Chernomyrdin, K. I. Zaytsev, and D. S. Ponomarev, Semicond. Sci. Technol. **34**, 034005 (2019).

45. A. E. Yachmenev, D. V. Lavrukhin, I. A. Glinskiy, R. A. Khabibullin, R. R. Galiev, A. Yu. Pavlov, Yu. G. Goncharov, I. E. Spektor, M. Ryzhii, T. Otsuji, K. I. Zaytsev, and D. S. Ponomarev, EPJ Conf. Series. **195**, 02009 (2018). https://doi.org/10.1051/epjconf/201819502009

46. E. R. Brown, K. A. McIntosh, K. B. Nichols, and C. L. Dennis, Appl. Phys. Lett. **66**, 285 (1995). https://doi.org/10.1063/1.113519

47. J. Y. Suen, W. Li, Z. D. Taylor, and E. Brown, Appl. Phys. Lett. **96**, 141103 (2010). https://doi.org/10.1063/1.337440

48. C. A. Balanis, *Antenna Theory: Analysis and Design,* 3rd ed. (Wiley-Blackwell, 2005).

49. S. Hava and M. Auslender, J. Appl. Phys. **73**, 7431 (1993).